



HAL
open science

Charging of ice-vapor interfaces: applications to thunderstorms

J. Nelson, Mark D. Baker

► **To cite this version:**

J. Nelson, Mark D. Baker. Charging of ice-vapor interfaces: applications to thunderstorms. *Atmospheric Chemistry and Physics*, 2003, 3 (4), pp.1237-1252. hal-00295319

HAL Id: hal-00295319

<https://hal.science/hal-00295319>

Submitted on 18 Jun 2008

HAL is a multi-disciplinary open access archive for the deposit and dissemination of scientific research documents, whether they are published or not. The documents may come from teaching and research institutions in France or abroad, or from public or private research centers.

L'archive ouverte pluridisciplinaire **HAL**, est destinée au dépôt et à la diffusion de documents scientifiques de niveau recherche, publiés ou non, émanant des établissements d'enseignement et de recherche français ou étrangers, des laboratoires publics ou privés.

Charging of ice-vapor interfaces: applications to thunderstorms

J. Nelson¹ and M. Baker²

¹Nelson Scientific, 7-13-8 Oginosato Higashi, Otsu, Shiga 520-0248, Japan

²Depts of Earth and Space Science and Atmospheric Sciences, University of Washington, Seattle, WA 98195-1310 USA

Received: 11 September 2002 – Published in Atmos. Chem. Phys. Discuss.: 6 January 2003

Revised: 8 May 2003 – Accepted: 25 July 2003 – Published: 28 August 2003

Abstract. The build-up of intrinsic Bjerrum and ionic defects at ice-vapor interfaces electrically charges ice surfaces and thus gives rise to many phenomena including thermo-electricity, ferroelectric ice films, sparks from objects in blizzards, electromagnetic emissions accompanying cracking in avalanches, glaciers, and sea ice, and charge transfer during ice-ice collisions in thunderstorms. Fletcher's theory of the ice surface in equilibrium proposed that the Bjerrum defects have a higher rate of creation at the surface than in the bulk, which produces a high concentration of surface D defects that then attract a high concentration of OH⁻ ions at the surface. Here, we add to this theory the effect of a moving interface caused by growth or sublimation. This effect can increase the amount of ionic surface charges more than 10-fold for growth rates near 1 $\mu\text{m s}^{-1}$ and can extend the spatial separation of interior charges in qualitative agreement with many observations. In addition, ice-ice collisions should generate sufficient pressure to melt ice at the contact region and we argue that the ice particle with the initially sharper point at contact loses more mass of melt than the other particle. A simple analytic model of this process with parameters that are consistent with observations leads to predicted collisional charge exchange that semiquantitatively explains the negative charging region of thunderstorms. The model also has implications for snowflake formation, ferroelectric ice, polarization of ice in snowpacks, and chemical reactions in ice surfaces.

1 Introduction

Electrical charging at the ice-vapor interface is revealed directly by surface potentials (Caranti and Illingworth, 1980) and high surface conductivities (Maeno, 1973), as well as being revealed indirectly by processes involving triboelectrification (Petrenko and Colbeck, 1995), ferroelectricity (Iedema et al., 1998), crystal growth (Rydock and Williams, 1991), temperature gradients (Jaccard, 1964), creation of new surfaces (Fifolt et al. 1992), and electrical attraction of ice crystals to other surfaces (Ohtake and Suchanek, 1970). Such charging can cause ice crystals to orient (Vonnegut, 1965) and possibly levitate (Gibbard et al., 1995) in the electrical atmosphere of thunderclouds. Surface charging can modify many atmospheric processes such as collection of ions, aerosols, and droplets by ice (Martin et al. 1980; Pruppacher and Klett, 1980 p. 619), and aggregation of snow crystals in clouds (Odenkrantz and Buecher, 1967; Finnegan and Pitter, 1988) and in wind-blown snow (Schmidt, 1982). The transfers of charge when an ice particle strikes another ice surface or another material are examples of contact charging involving electronic insulators, one of the oldest problems of an electrical nature (Castle, 1997). For example, static discharges occur when snow particles recoil from wires and aircraft (Ives, 1938; FAA, 2001). But the most spectacular outcome of the contact charging of ice occurs in thunderstorms when mm-sized ice particles formed from accreted supercooled drops, hereafter graupel, fall at speeds exceeding 5 m s^{-1} and strike small, uplifting ice crystals (Illingworth, 1985). About 20 fC per collision is transferred from one to the other, leading to powerful in-cloud electric fields and often lightning, thus maintaining Earth's electrical circuit. We present a simple analytic model that is consistent with these wide-ranging observations and which allows speculation that the same processes can lead to lightning on Jupiter (Gibbard et al. 1995) and elsewhere in the solar system.

Correspondence to: J. Nelson
(nelson@sd5.so-net.ne.jp)

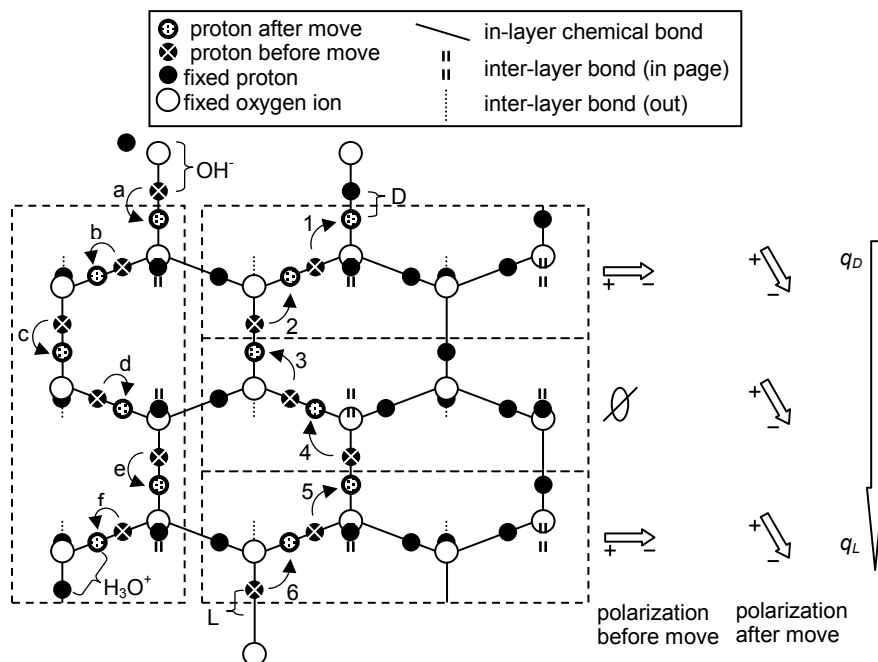


Fig. 1. Idealized sketch of fundamental charging processes in an ice lattice. The three dashed, stacked boxes on the right show the creation of a D and L defect by the rotation of an H_2O molecule and the subsequent downward migration of the L along a prism plane of ice. Before step 1, “fixed protons” and “protons before move” produce net dipole moments that are neither up nor down in all three boxes as shown to the right (e.g., compare protons above and below a horizontal line in the middle of a box). After step 1, the top bond has a D defect (2 protons) and the bond below and left has an L defect (no protons). Step 2 moves a proton to the empty bond created by step 1 thus moving the L defect down. After 6 such moves, all three boxes have net polarization pointing down. Thus, the ice effectively has net positive charge q_D on top and negative charge on bottom; this holds even if, as theory predicts, the 2 protons in a D defect are not collinear and the defects distort the lattice. (Indeed, the middle and lower boxes would be polarized even if the D was not present.) The dashed, vertical box on the left shows the creation of an OH^- and H_3O^+ by the shift of a proton along a hydrogen bond (step a) and the subsequent downward migration of H_3O^+ in b–f. Inspection of the latter path of bonds shows that the passage of H_3O^+ through the lattice also polarized the lattice. For this reason, the effective charge of OH^- in ice q_{OH} is $-0.62e$, not e .

2 Physical basis and approach

Jaccard (1964) developed a microscopic theory of the electrical properties of ice that uses the conservation equations for ions OH^- and H_3O^+ and Bjerrum D and L defects to explain ice thermoelectricity with and without impurities. D and L defects, which are respectively double and empty bonds between H_2O molecules, are the majority charge carriers in bulk ice and are responsible for the fact that ice’s static relative permittivity exceeds 100 below 0°C . Unlike the ions, the Bjerrum defects create internal electric fields via their polarization of the ice lattice as they migrate such that the D defect effectively has a positive charge and L is negative (Fig. 1). Because D and L charges arise from rotations of H_2O molecules that violate the ice rules, they are not free charges and cannot transfer charge in collisions. However, because their bulk concentrations are about 10^6 times those of the water ions at equilibrium (Petrenko and Whitworth, 1999; hereafter PW, pg. 154), they greatly influence the electric field inside ice. This is supported by experimen-

tal evidence that suggests Bjerrum defects are important for ice surface charging: collisional charge exchange, presumably due to OH^- , increases with ice crystal growth rate even though surface potential measurements, which would detect the neutralization between the OH^- and D, have little dependence on growth rate (Caranti and Illingworth, 1980). The same surface potential measurements show the ice-vapor interface to be positive, which would not occur if the surface contained only OH^- .

Our model is built on the fundamental physical ideas of Jaccard theory but is not sensitive to the molecular structure of Bjerrum defects; we require only their effective charges and mobilities that have been inferred from numerous experiments summarized in PW (pg. 154). Because the ice-vapor interface has anomalous structural and electrical properties, Jaccard’s model must be supplemented with a description of the surface. The oft-used surface disorder theory in Fletcher (1968) predicts that the surface region has a low activation energy for the creation of D and L. According to Fletcher, forces from dipole-quadrupole interactions push

Table 1a. Relevant electrical properties of ice

#	Experimentally established property
1	A high static relative permittivity*.
2	Thermoelectric effect [†] .
3	High surface dc conductivity in equilibrium [‡] .
4	Interior ionic charge separation Q over entire crystal during growth [§] .
5	Surface potential insensitive to vapor growth or sublimation ^{††} .
6	Surface dc conductivity increases during sublimation [‡] .
7	Q greater during growth than in equilibrium ^{**} .

* Johari (1981) and references therein.

[†] Jaccard (1964)

[‡] Maeno (1973)

[§] Inferred from the frost growth experiments of Rydock and Williams (1991), Dong and Hallett (1992), and Latham (1963). These experiments indicate an excess of OH^- at the surface for growing frost and an excess of H_3O^+ at the surface during sublimation.

^{††} Caranti and Illingworth (1980)

** Williams et al.'s (1991) interpretation of Latham's (1963) experiments.

Table 1b. Relations of charge transfer to graupel ΔQ from laboratory experiments

#	Observed relation explained by the model
1	ΔQ mostly independent of physical properties of the flatter surface [†] .
2	$\Delta Q \propto U^\dagger$.
3	Variable ΔQ under same conditions; $\Delta Q < 0$ even occurs in $\Delta Q > 0$ regime [†] .
4	$\Delta Q \propto D^m$ with $m=2$ for spheres [†] , $m \approx 0.6-0.8$ for vapor-grown ice*.
5	ΔQ peaks near $T = -15^\circ\text{C}$ for vapor-grown crystals [‡] .
6	In equilibrium, ΔQ smaller for vapor-grown ice crystals than for spheres [§] .
7	$\Delta Q > 0$ when vapor-grown ice crystals are sublimating ^{††} .
8	For $T < -10^\circ\text{C}$, $\Delta Q < 0$ regime for $\rho_l \approx 0.3 - 3 \text{ g m}^{-3}$, $\Delta Q > 0$ regime at other ρ_l [‡] .
9	ΔQ increases for ice doped with NH_3 , but reverses sign with HF doping ^{**} .

Based on experiments with ice spheres ($r_{1p} = R_{cr} = D/2$) and vapor-grown ice ($r_{1p} \ll R_{cr} < D/2$) impacting graupel. D is the maximum crystal dimension, U is the impact speed, and T is the ambient temperature. In relation #s 5 and 8, the experimental clouds had cloud liquid water of density ρ_l ; in all others, $\rho_l \sim 0$.

[†] GI (relation #s 1, 2, 3, 4) and Marshall et al. (1978) (relation #s 1, 2, 3) for $\Delta Q < 0$ regime and data in Illingworth and Caranti (1985) (relation #1).

* Keith and Saunders (1990)

[‡] Takahashi (1978) (relation #s 5 and 8) and Berdeklis and List (2001) (relation #5)

[§] Compare data in GI to reports of almost no charging when only vapor-grown crystals strike graupel (i.e., $\rho_l \approx 0$ so $v=0$ in Takahashi, 1978 and Baker et al., 1987)

^{††} Saunders et al. (2001)

** Buser and Aufdermaur (1977)

the D defects to the outermost surface layer where their protons point out of the surface and similarly push L defects inward. This surface polarization pulls OH^- ions to the surface thus leading to a high surface dc conductivity. Petrenko and Ryzhkin (1997), hereafter PR, argue that the surface traps D defects, which is consistent with Fletcher's result. The fit of the PR model to the measured surface potential and surface conductivities predicts equilibrium surface concentrations of

Bjerrum and ionic defects that are respectively 10^6 and 10^{11} times the bulk concentrations.

Many attempts have been made to explain the charging of ice during growth and the subsequent contact charging during collisions. Several of these invoke the fact that the H_3O^+ ion is much more mobile than OH^- in ice (Jaccard, 1964; PW, p. 154), so that charge separation occurs when the ions move down concentration or field gradients at different rates.

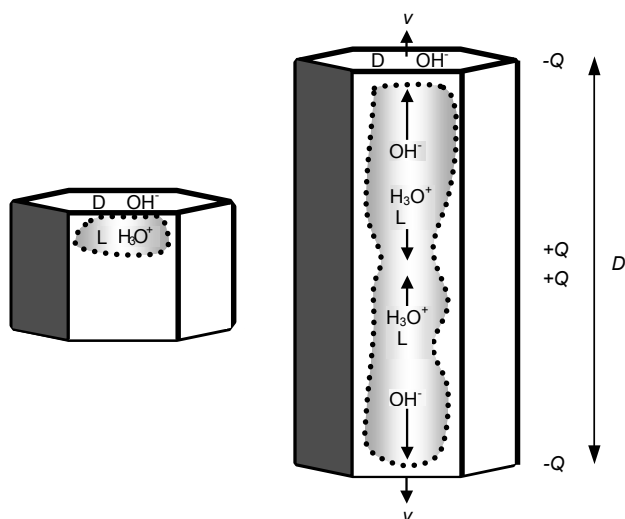


Fig. 2. Concentrated charge regions within ice without growth or sublimation (“equilibrium” on left) and during growth at speed v (right). (Dotted lines frame imaginary “windows” to the ice interior.) In equilibrium, the interior L and H_3O^+ charges are very near the surface (left; only charges on top surface shown), whereas they are effectively driven towards the crystal center during growth (right). Growth also increases surface D and OH^- as described in the text. Net ionic charge Q and maximum crystal size D are marked on the right.

But we focus here on two new aspects to this problem. One is a “sweeping” effect caused by the moving ice surface when ice grows or sublimates (an example of a “Stefan” moving boundary problem), which can increase or decrease the negative surface charge depending on whether growth or sublimation occurs. The second aspect is the well-known property of ice to melt under pressure: when the corner of an ice crystal strikes another surface, the force of the collision can produce melt that is then pushed to the side, due to the pressure gradient, and onto the graupel. This process transfers charge to the graupel, leading to large-scale charge separation in thunderclouds. However, the complex ice-atmospheric environment in nature and in experiments makes it difficult to quantitatively compare theory to most ice-charging-related studies. Nevertheless, we use the model to explain the more reliable trends that are listed in Tables 1a and b. Furthermore, we use measured ice crystal vapor growth rates and reasonable estimates of two collision parameters to show that our model semi-quantitatively agrees with experiments that simulate thunderstorm charging.

3 Surface charging during growth or sublimation

We assume the ionic and Bjerrum carriers are created and recombined in pairs and migrate in the ice. To treat both “equilibrium” (stationary surface) and nonequilibrium (mov-

ing surface), we write the equations in a reference frame moving with the surface at speed v , where v is positive, negative, or zero corresponding to growth, sublimation, or equilibrium. Thus, when $v > 0$, even without the defects hopping between lattice sites, there is an effective flux of defects towards the ice interior. This “sweeping” flux is $vd(x)$ for D, where $d(x)$ is the number concentration of D. $d(x)$ obeys the following continuity equation with x being the distance from the surface:

$$\partial d / \partial t = F_B - dl / (\langle l \rangle \tau_B) - \partial j_D / \partial x, \quad (1)$$

where F_B is the creation rate of Bjerrum D and L pairs, $l(x)$ is the L concentration with bulk average $\langle l \rangle$, τ_B is the time scale for D and L to recombine to reach steady state, and j_D is the number flux of D into the crystal. The units and approximate values of all symbols are in Appendix A. Because D is much less mobile than the other three defects (PW, p. 154), we simplify the problem by assuming D is immobile. Thus, $j_D = vd$. For the other three defects, the flux includes diffusion and drift in an electric field E . In particular, the concentration h^- of the OH^- ion follows

$$\partial h^- / \partial t = F_I - h^- h^+ / (\langle h \rangle \tau_I) - \partial j_{\text{OH}} / \partial x \quad (2)$$

with

$$j_{\text{OH}} = -D_{\text{OH}} \partial h^- / \partial x - \mu_{\text{OH}} E h^- + v h^-, \quad (3)$$

where D_{OH} is the diffusion constant, μ_{OH} is the mobility of OH^- , and E is the electric field. Similar equations hold for the L defects and H_3O^+ ion concentration h^+ with the obvious substitutions.

Because the mobilities of all four defects are included, the model is consistent with the high static relative permittivity of ice. Moreover, numerical solutions of the equations for macroscopic pieces of ice (not shown) agree well with the thermoelectric effect in pure ice. Thus, this model is consistent with entries 1–2 of Table 1a. Following Fletcher, we assume a low activation energy of D and L at the surface, which results in an excess of surface D over L that attracts a high concentration of OH^- to the surface (Fig. 2) thus producing a high dc surface conductivity (entry 3, Table 1a).

The bulk concentrations $\langle d \rangle$ and $\langle l \rangle$ of defects D and L are about 10^6 times the bulk ion densities. Hence, in the bulk, a change of D or L by only $10^{-4}\%$ would create an electric field that is comparable to that of a change of OH^- or H_3O^+ by 100%. Thus, we focus first on D and L, and then assume the ions respond to the E -field perturbation δE created by the change in D and L. This is analogous to Fletcher’s approach to estimate the ionic charging of the ice surface. More importantly, the assumptions allow us to construct a simple analytic model that preserves the basic physical properties of the charge transfer mechanism, and, as we show below, the model is in semi-quantitative agreement with observed charge transfer trends. In steady state, Eq. (1) predicts

$$vd' = F_B - dl / (\langle l \rangle \tau_B). \quad (4)$$

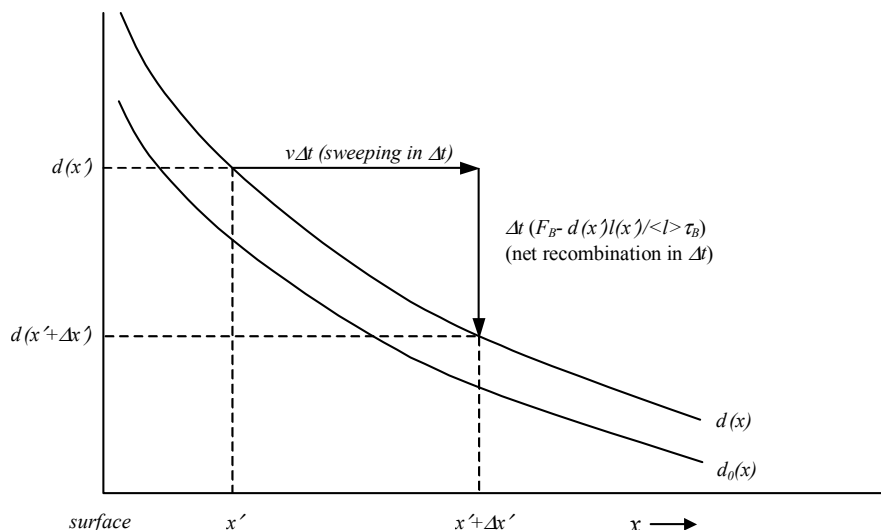


Fig. 3. Mechanism by which creation-recombination and the sweeping flux due to growth increases the D concentration $d(x)$ near the surface. In time Δt growth adds a layer of thickness $v\Delta t$, thus effectively sweeping charge $d(x')$ at point x' a distance $\Delta x' = v\Delta t$ from the surface. In this time, net recombination removes an amount $\Delta t(F_B - d(x')l(x')/\langle l \rangle \tau_B)$.

Thus, creation-recombination balance does not occur during growth. Even when v is very small, the product on the LHS of Eq. (4) can be significant because d' would roughly equal the equilibrium value d'_0 , which is very large near the surface.

The equilibrium concentration $d_0(x)$ decays rapidly with distance x (PR). For simplicity, we assume

$$d_0(x) = d_0(0) \exp[-x/\Delta_D], \quad (5)$$

where the length scale Δ_D is expected to be much less than $1 \mu\text{m}$. We also assume $l(x) = \langle l \rangle$. Later, we will show that this assumption underestimates the charging. The advantage of this assumption is that it allows us to avoid solving a nonlinear, integro-differential equation. Assuming $d(x) = a \exp[-x/\Delta_D]$ and solving for a ,

$$d(x) = d_0(0) \exp[-x/\Delta_D] / (1 - v\tau_B/\Delta_D). \quad (6)$$

Thus, the charge profile due to growth or sublimation δd is

$$\begin{aligned} \delta d(x) &\equiv d(x) - d_0(x) \\ &= -v\tau_B d'_0(x) / (1 - v\tau_B/\Delta_D), \end{aligned} \quad (7)$$

where the latter equality follows from Eq. (5). Hereafter, all deviations from equilibrium are represented by the symbol δ . Physically, $\delta d(x) > 0$ at the surface during growth because the advancing surface effectively “sweeps” surface D inward ($d'(0) < 0$ at the surface), and thus $d(x)$ must increase until the recombination rate balances this effective flux (Fig. 3). A distinctive and important property of sweeping (i.e., vd , vl) is its action on all parts of a crystal; growth pushes L towards the crystal center as D builds up near the surface. This large-scale polarization sets up an electric field that pulls more

OH^- ions to the surface and pushes H_3O^+ ions towards the crystal center (Fig. 2) in accord with entry 4 in Table 1a. The opposite occurs during sublimation.

By integrating $\delta d(x)$ over x , the total D charge per area $\delta\sigma_D$ is

$$\delta\sigma_D = -q_D v \tau_B d_0(0) / (1 - v\tau_B/\Delta_D), \quad (8)$$

where q_D is the effective charge on the D defect. To estimate τ_B we used a simple electrostatic model to estimate how rapidly a lone L defect is pulled to an immobile D defect. Without giving the details, we just state the result here:

$$\tau_B \approx 6\epsilon_0\epsilon_\infty / \mu_L q_L \langle l \rangle, \quad (9)$$

where μ_L is the mobility of L with effective charge q_L and ϵ_∞ is the high-frequency permittivity. Using recommended values in the appendix, $\tau_B \approx 4.6 \times 10^{-5} \text{ s}$ at $T = -20^\circ\text{C}$. With this τ_B and $\Delta_D > 3 \times 10^{-10} \text{ m}$ (~ 1 crystal layer), the denominator in Eqs. (7) and (8) are about 1 for any vapor growth speed v in the atmosphere. Hereafter, we assume the denominator is unity.

The distribution of perturbed OH^- charge δh^- at the surface is also important. To estimate the thickness of the OH^- region that forms in response to $\delta\sigma_D$, we assume that the perturbed OH^- flux $\delta j_{\text{OH}^-} = v h^-$, a relation that is exact at the surface but is of unknown accuracy in the interior. Thus, from Eq. (3)

$$D_{\text{OH}^-} \partial \delta h^- / \partial x = -\mu_{\text{OH}^-} \delta E \delta h^-, \quad (10)$$

where the electric field due to the non-equilibrium charges $\delta\sigma_D$ and δh^- is

$$\delta E(x) = \delta\sigma_D / \epsilon_0 \epsilon_s - (q_{OH} / \epsilon_0 \epsilon_s) \int_0^x dy \delta h^-(y). \quad (11)$$

Near the charged layer $\delta\sigma_D(x \sim 0)$, the second term on the right side of Eq. (11) can be neglected. Thus, near the surface, Eq. (10) gives

$$\partial \delta h^- / \partial x \approx -\delta h^- / \Delta_{OH}, \quad (12)$$

where $\Delta_{OH} \equiv D_{OH} \epsilon_0 \epsilon_s / \mu_{OH} \delta\sigma_D$. For a typical vapor growth rate of $0.1 \mu\text{m s}^{-1}$ at -20°C , $\Delta_{OH} \sim 0.04 \mu\text{m}$, which is much thinner than the mass-loss regions we estimate in Sect. 4.

The surface potential caused by nonequilibrium $\delta\phi_{surf}$ is approximately $\delta E \Delta_{OH}$. Equation (12) suggests that $\delta\phi_{surf}$ is independent of growth rate; as charging increases, the OH^- charges simply move closer to the D defects. Indeed, $\delta E(0) \Delta_{OH} \approx D_{OH} / \mu_{OH} \approx kT / q_I = 36 \text{ mV}$ using Eq. (11), the Einstein relation between diffusivity and mobility, and the values in the appendix. Thus, the model is consistent with the observations (Caranti and Illingworth, 1980) showing that $\delta\phi_{surf}$ varies by only 25 mV over a range of temperatures and growth rates even though collisional charging measurements (Baker et al. 1987; Berdeklis and List, 2001) indicate that the ionic charging increases with growth rate (entry 5, Table 1a).

To estimate the nonequilibrium ionic surface charge $\delta\sigma$ we consider how much OH^- screens the $\delta\sigma_D$ layer. For this, we compare the drift speed $\mu_{OH} \delta E(x)$ of OH^- ions near the high-D surface layer ($x \sim 0$) to the drift speed near the crystal center at $x \sim D/4$. To make the discussion specific, assume $v = 0.1 \mu\text{m s}^{-1}$ and $T = -20^\circ\text{C}$. For $x \sim 0$, $\delta E = \delta\sigma_D / \epsilon_0 \epsilon_s \sim 0.95 \times 10^6 \text{ V m}^{-1}$, which results in an estimated drift speed of $\sim 2.8 \times 10^{-2} \text{ m s}^{-1}$, using the values in the appendix. Moving closer to the center of the crystal at $x \sim D/4$, h^- decreases and becomes uniform. Here, the diffusive flux vanishes. Thus, assuming $\delta j_{OH} = 0$, the electric field must be just enough for the drift speed $\mu_{OH} \delta E$ to balance the sweeping speed $v = 0.1 \mu\text{m s}^{-1}$. That is, $\mu_{OH} \delta E(D/4) \sim 0.1 \mu\text{m s}^{-1}$. For this to occur, $\delta E(x)$ must decrease from its near surface value by a factor of 2.8×10^7 (the ratio of the drift speeds). Therefore, practically all of the charge $\delta\sigma_D$ must be screened by negative charge. Consistent with our assumption that OH^- and H_3O^+ respond to growth perturbations of L and D, we assume this screening charge is OH^- , not L. Moreover, the OH^- mobility is likely greater than that of L for most relevant atmospheric temperatures (Bryant, 1967; PW, p. 154) and thus would more readily screen $\delta\sigma_D$. Thus,

$$\delta\sigma \approx \delta\sigma_D = -q_D v \tau_B d_0(0) \quad (13)$$

is the additional ionic charging due to growth or sublimation.

During sublimation, $v < 0$ and hence d decreases as l increases at the surface. This pulls H_3O^+ to the surface. Because the dc surface conductivity is proportional to mobility times surface concentration, the increased concentration of the highly-mobile H_3O^+ during sublimation should increase the dc surface conductivity. This agrees with measurements (entry 6, Table 1a).

Even though the effective ionic charge within the ice is $\pm 0.62e$, each surface ion transferred in a collision carries a charge of $\pm e$. Thus, we use here an ionic surface charge density σ that is e times $(h^+ - h^-)$ integrated over the surface region. During growth, the surface removes H_3O^+ from the surface region; hence, in this case we neglect h^+ and thus

$$\sigma = \sigma_0 + (e/q_{OH}) \delta\sigma, \quad (14)$$

where σ_0 is the equilibrium ionic surface charge density. PW (p. 238) estimated $|\sigma_0| \sim 10^{-4} - 10^{-3} \text{ C m}^{-2}$, which is smaller than the calculated values of $(e/q_{OH}) |\delta\sigma|$. In particular, $(e/q_{OH}) |\delta\sigma| = 2.4 \times 10^{-3}$, 1.3×10^{-2} , and $8.6 \times 10^{-2} \text{ C m}^{-2}$ for -10 , -20 , and -30°C , respectively, for a growth rate of $1 \mu\text{m s}^{-1}$. This large increase of charging during growth helps explain entry 7 in Table 1a.

To summarize: the D defects build up during growth, while the L do not, because of the lower mobility of the D; in particular, the D are swept into the crystal with flux vd faster than they can diffuse back to the surface. Equation (1) shows that when growth first starts, $\partial d / \partial t \approx -vd'_0 > 0$ at the surface. Conversely, $\partial l / \partial t \approx -vl'_0 < 0$ because $l'_0 > 0$ according to the analysis in PR. Thus, growth causes d to increase at the surface and l to decrease. The same argument shows that d decreases while l increases during sublimation.

The success of this model at explaining observations in Table 1a lends confidence to its application to the more difficult case of ice-ice collisions.

4 Charge transfer during ice-ice collisions

An obvious manifestation of large-scale charge separation is lightning, which is thought to depend partly on net transfer of electric charge during ice-ice collisions (Illingworth, 1985). In well-characterized experiments on ice-ice collisional charging, sub-millimeter, freshly-frozen, mono-dispersed ice spheres near equilibrium collided with a larger ice surface, and induction rings tracked the charge on the spheres before and after impact (Gaskell and Illingworth, 1980; hereafter GI). When the target ice was not growing, the charge transfer ΔQ was roughly independent of the temperature and doping of the target. Other experiments support the latter finding (Illingworth and Caranti, 1985) but also show that the charging depends on the doping in the sub-millimeter ice sphere. Similarly, Marshall et al. (1978) found that the target charged negatively when it was warmer than the ice sphere, but the magnitude was independent of the target temperature when this difference exceeded 1.5°C . The

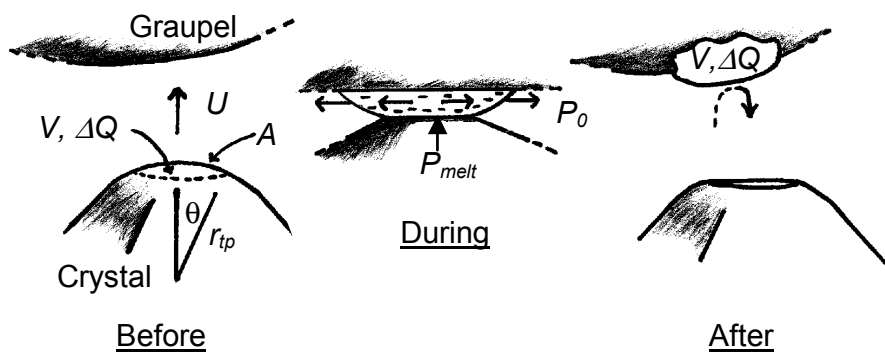


Fig. 4. Mass and charge transfer from the corner of a faceted crystal to the underside of sublimating graupel. The graupel surface is assumed flat over regions of order $15\ \mu\text{m}$. $P_0 (\ll P_{\text{melt}})$ is atmospheric pressure. Before the collision, the crystal surface has OH^- with charge density σ (Eq. 14) and total charge ΔQ . The collision squeezes this charged mass into melt (exaggerated here) that is pushed outward from a thin region between the ice particles and then freezes onto the graupel. For θ below about 0.61, $A \sim \pi r_{\text{tp}}^2 \theta^2$, $V \sim \pi r_{\text{tp}}^3 \theta^4 / 4$, and the maximum thickness of the transferred volume before the collision is $(V/\pi r_{\text{tp}})^{0.5}$.

lack of influence from the properties of the target ice surface is inconsistent with surface state theory (e.g., Castle, 1997) that has been successfully applied to the contact charging of other materials. We argue below that this unusual property of charging during ice-ice collisions, as well as the other observed relations in Table 1b, arise from a primarily one-way transfer of charged melt.

Experiments by Mason and Dash (2000) found that negative charge transfer between contacting ice surfaces is correlated with a mass transfer, and subsequent analysis indicated that the mass is likely melt (Dash et al., 2001). Pressure melting can explain this finding. In particular, the maximum pressure P_{con} at the contact area during elastic rebound of a small ice crystal on a flat ice surface is (Higa et al., 1998)

$$P_{\text{con}} = 1.95 \times 10^8 (R_{\text{cr}}/r_{\text{tp}})^{0.6} U^{0.4}, \quad (15)$$

where R_{cr} is the equivalent sphere radius of the smaller crystal, r_{tp} is its radius of curvature at the initial point of contact (Fig. 4), and U is its impinging speed normal to the surface. We fit Kishimoto and Maruyama's (1998) data on the melting pressure of ice P_{melt} to

$$P_{\text{melt}} = -1.224 \times 10^7 T - 1.171 \times 10^5 T^2, \quad (16)$$

for temperature T [$^{\circ}\text{C}$] between 0 and -24°C . For a given T , equating P_{con} to P_{melt} determines a critical speed above which pressure melting can occur in the contact region. These critical speeds are much less than the updrafts in the strong electrical charging regions of thunderstorms, particularly when $r_{\text{tp}} \ll R_{\text{cr}}$ (Table 2). Hence, elasticity theory indicates that pressure melting occurs for typical ice-ice collisions in clouds. Collisional forces change dramatically once melt forms, so the theory by itself cannot predict the amount of melt transfer. To estimate this quantity, we use a cruder approach.

Just before contact, the ice surface on the two particles may be at different temperatures, have different charge densities, and different radii of curvature. In some experiments, for example those of Latham and Mason (1961) and Mason and Dash (2000), the two contacting ice surfaces likely had nearly equal radii of curvature. The theories of Latham and Mason (1961) and Dash et al. (2001), respectively, can explain these experiments. However, their theories poorly explain other experimental data that are relevant to the atmosphere: charge transfer based only on temperature differences (Latham and Mason's) has been ruled out as the generator of thunderstorm electricity because it is too weak (Illingworth, 1985), and Dash et al.'s mechanism based on different surface charge densities and temperatures between the two surfaces does not explain measured charge transfers during collisions between two nongrowing crystals (GI). In contrast, the initial points of contact between colliding atmospheric ice particles should usually have very different radii of curvature. We argue here that, in most atmospheric situations, the estimated direction of mass transfer is dominated by the difference in radii of curvature between the particles.

When contact occurs, the pressure builds up until melt forms. This melt can form on both particles in the contact region; however, the melt that forms in the initially sharper particle has a much stronger horizontal pressure gradient forcing the fluid to the side and thus to the flatter particle (Fig. 4). If a slice of area a and thickness Δx melts and remains at $P_{\text{melt}}(T)$, the work to quasistatically push this fluid to the side is $P_{\text{melt}}(T)a\Delta x$. There will be local cooling caused by melting and heating due to viscous dissipation and refreezing, but for simplicity, we assume T remains at its original value. The total work to remove the melt from the sharper particle will be some fraction f of the incident kinetic energy KE of the collision. By summing the work for each slice of thickness Δx , $f\text{KE} = P_{\text{melt}}(T) \sum a\Delta x$. Thus, the

total transferred volume $V = \sum a \Delta x$ is

$$V = f 2\pi \rho_i R_{cr}^3 U^2 / 3 P_{melt}(T), \quad (17)$$

where ρ_i is the mass density of ice and f is the fraction of KE used to transfer mass. Dash et al. (2001) predict about 12-fold more melt volume than that in Eq. 17 because they neglect the work to push the melt aside. (Their neglect of horizontal melt flow may be reasonable for their experiments as the "collisions" repeatedly occurred in the same area, but in most other experiments and in the atmosphere, it is less likely to be accurate.) Because other processes, including some mass flow from flatter to sharper surface, can also remove KE from the collision, f is less than the inelasticity of the collision. Measurements with ice spheres (Higa et al., 1998) impacting normally on a flat ice surface show that the inelasticity increases with decreasing size and is ≈ 0.5 for $R_{cr} = 1.4$ mm. Thus, f could exceed 0.5 for atmospheric ice crystals if no other processes absorb KE, although $f \sim 0.02 - 0.2$ fits the charging measurements described below, which are likely averages over both normal and glancing collisions.

We now consider the atmospherically relevant situation, simulated in a number of lab experiments, in which a small pointed ice crystal impacts a broader graupel surface. In this case, V is the volume of ice in the crystal corner between the original point and a slice normal to the contact plane (Fig. 4). Thus, the original surface charge in this volume transfers and freezes to the flatter ice surface, which, unless otherwise stated, is assumed to be the graupel. When the graupel surface is very near the melting temperature and significantly warmer than the crystal, the graupel contact point could melt before that in the crystal and possibly reverse the overall direction of charged-mass transfer. Such a reversal of mass transfer might explain the positive graupel charging in Pereyra et al. (2000) when the graupel surface was above $\sim -7^\circ\text{C}$ and the crystals were about -10°C . (The temperature difference between the surfaces might also govern the overall direction of mass flow when the contact radii of both particles are large and nearly the same. But this situation should be relatively rare in the atmosphere.) Thus, in general, we assume that mass transfers from the sharper to the flatter (graupel) surface. This can explain entry 1 in Table 1b.

We briefly consider how other factors might also favor mass transfer to the flatter surface. For example, shearing off of the sharper point and partial penetration of the sharper point into the flatter surface favor mass loss of the sharper particle. Also, the sharper particle might melt more readily than the graupel because it might be softer. The relative softness can arise from frictional heating if it scrapes along the graupel and the charge itself can soften the ice corner due to electrostatic pressure according to PR. Finally, Sommer and Levin (2001) predicted significant amounts of mass transfer from sharp ice-crystal points to relatively-flat graupel due to asymmetries in the molecular interactions at the surfaces.

4.1 Charge transfer in equilibrium

We first use measured (GI) charge transfers for collisions between frozen droplets and relatively flat, nongrowing surfaces (simulated graupel) to fit f or σ_0 for the transfer of equilibrium charge ΔQ_0 . We then use the best-fit parameter to compare predicted with measured charge transfers during collisions of faceted growing crystals with graupel.

If the tip of the impacting crystal has radius of curvature r_{ip} and the mass transferred is V , then the surface area region that melts and transfers charge is $A \approx 2(\pi r_{ip} V)^{0.5}$. The resulting charge transfer is $\sigma_0 A$. Substituting for V from Eq. (17),

$$\Delta Q_0 \approx \pi \sigma_0 f^{0.5} U (8 \rho_i / 3 P_{melt})^{0.5} r_{ip}^{0.5} R_{cr}^{1.5}, \quad (18)$$

where $P_{melt}(T)$ is evaluated at the ambient temperature T . The fact that ΔQ_0 is proportional to U and not U^2 is due to the locally-spherical nature of the corner (Fig. 4). As $\Delta Q \propto A \propto U$, Eq. (18) agrees with entry 2 in Table 1b. To determine $\sigma_0 f^{0.5}$ in Eq. (18), we set $r_{ip} = R_{cr}$, $P_{melt} = 1.1 \times 10^8$ Pa ($T = 10^\circ\text{C}$), and then fit ΔQ_0 to the measurements in GI to obtain $\Delta Q \approx -6.4 \times 10^{-7} U R_{cr}^2$. The result is $\sigma_0 f^{0.5} = -4.3 \times 10^{-5} \text{ C m}^{-2}$ and thus $f = 0.16$ for an estimated equilibrium σ_0 of $-10^{-4} \text{ C m}^{-2}$ (PW, pg. 238). This fit for the data also agrees well with Buser and Aufdermaur's measurements at -45°C for $R_{cr} = 10 \mu\text{m}$ and $U = 10 \text{ m s}^{-1}$: using $P_{melt} = 380$ MPa, the predicted charge is $\Delta Q = -0.32$ fC versus the measured value of -0.3 fC. Thus, Eq. (18), with constant $\sigma_0 f^{0.5}$, appears useful over a wide radius and temperature range.

However, in the atmosphere, collisions involve vapor-grown ice crystals and graupel, both of which are nonspherical. Vapor-grown ice crystals generally have flat, faceted faces separated by sharp edges and corners, whereas the surface of graupel is generally knobbly but can have frost or liquid water. In the absence of some presently unknown alignment force, all collisions should involve the corner of one particle striking a relatively flat section of the other particle. The shape at a crystal corner should be approximately spherical and the resolution in ice crystal photographs suggests that $r_{ip} < 5 \mu\text{m}$. Conversely, graupel surfaces grow when drops of diameter typically exceeding $15 \mu\text{m}$ impact, flatten, and freeze. Thus, when graupel does not have frost, the graupel likely has the flatter surface in most collisions and hence would receive the charged mass from the crystal. However, as there is considerable variation possible in impact orientation and local shape on a graupel surface, significant variation in ΔQ is predicted; this variation should be particularly large when the graupel has frost or fragile rime branches, which agrees with experiment (entry 3, Table 1b).

4.2 Nonequilibrium charge transfer

During growth or sublimation, the total ionic charge density at the interface σ is $\sigma_0 + (e/q_{OH})\delta\sigma$, where $\delta\sigma$, the growth

Table 2. Collision speed U [m s^{-1}] above which pressure melting can occur in ice crystal collisions

R_{cr}/r_{tp}	T[°C] collision type	−5	−10	−15	−20	−25
1	ice sphere-flat ice	4.9×10^{-2}	2.5×10^{-1}	5.9×10^{-1}	1.0	1.6
10	snow-flat ice	1.6×10^{-3}	7.8×10^{-3}	1.9×10^{-2}	3.3×10^{-2}	5.0×10^{-2}
10	snow-snow	2.2×10^{-3}	1.1×10^{-2}	2.6×10^{-2}	4.7×10^{-2}	7.0×10^{-2}
10	snow-metal	3.9×10^{-4}	1.9×10^{-3}	4.6×10^{-3}	8.3×10^{-3}	1.2×10^{-2}
10	snow-rubber	2.4×10^4	1.2×10^5	2.9×10^5	5.2×10^5	7.8×10^5

Values from Eqs. (15) and (16). The snow-snow collision is for tip-to-center collisions between two ice crystals of the same mass and follows by replacing R_{cr}^3 with $0.5 R_{cr}^3$ in Eq. (15). The bottom two rows apply to snow crystals striking large, flat surfaces of the listed material; metal refers to any material with Young's modulus greatly exceeding that of ice (9.33 GPa), and the estimates for rubber assumed a Young's modulus of 1 MPa.

increment, is given by Eq. (13). When σ_0 in Eq. (18) is replaced by σ , the total charge transfer to the graupel ΔQ becomes

$$\begin{aligned} \Delta Q &= \Delta Q_0 + \Delta Q_v \\ &= - (K_0 + v f^{0.5} K_1) U r_{tp}^{0.5} R_{cr}^{1.5} P_{melt}^{-0.5}, \end{aligned} \quad (19)$$

where

$$K_0 \equiv \pi (8\rho_i/3)^{0.5} |\sigma_0| f^{0.5}, \quad (20)$$

and

$$K_1 \equiv \pi (8\rho_i/3)^{0.5} e(q_D/q_{OH}) d_0(0) \tau_B. \quad (21)$$

Inserting the above fit for $\sigma_0 f^{0.5}$ and numerical values for the other parameters from the appendix, $K_0 = 6.7 \times 10^{-3}$ and $K_1 = 2.1 \times 10^6 \exp[1.14 \times 10^4 (1/T[K] - 1/253.15)]$. The temperature dependence of K_1 is from τ_B . (Temperature dependences of K_0 and other factors in K_1 are presently unknown.)

In the charge transfer literature, crystal size is usually given in terms of maximum crystal dimension D . However, because ice crystals change shape during growth, R_{cr} is not proportional to D ; rather, for up to 5-min of growth, measurements find $R_{cr}^3 \propto D^{1.7}$ for tabular crystals and $R_{cr}^3 \propto D^{1.03}$ for columnar crystals (Takahashi et al., 1991). Collision experiments (Keith and Saunders, 1990) with vapor-grown crystals impacting a stationary ice target at -25°C and $U = 10 - 50 \text{ m s}^{-1}$ showed that $\Delta Q \propto D^{0.6-0.8}$. With this growth data, Eq. (19) predicts $\Delta Q \propto D^{0.5-0.9}$ (including both columnar and tabular cases), which agrees well with measurement (entry 4 in Table 1b). Most importantly, for reasonable parameter values, Eq. (19) quantitatively agrees with collision experiments under simulated thunderstorm conditions as shown in Fig. 5. The predicted peaks in the charging near -14.4°C are due to the peaks in v and R_{cr} at this temperature (entry 5, Table 1b). Thus, the variation in growth rate dominates the temperature trend, a factor that has not been explicitly realized in previous models of the charge

transfer but is consistent with the oft-stated hypothesis from Baker et al. (1987): “The faster-growing particles (by vapor transfer) acquire positive charge”. Other trends are apparent. For example, lower temperatures have larger charging mainly because of the larger relaxation time τ_B at low temperatures. Also, larger radii of curvature r_{tp} at the contact point have greater charging because of the greater surface area (which can explain entry 6 in Table 1b), and a larger collision efficiency f results in more charging because more ice melts. Finally, we mention that previous charging theories have difficulty explaining the positive charging of graupel when the ice crystals are sublimating (Saunders et al., 2001); but such charging follows from Eq. (19) because $v < 0$ and $K_1 \gg K_0$. This can explain entry 7 in Table 1b.

5 Further implications of charge transfer model for thunderstorm electrification

5.1 Thunderstorms

In thunderstorms, the collision speed U and the colliding ice particles' masses and growth rates all increase, in general, with increasing updraft speeds. Thus, our model helps explain why fast updraft speeds and rapid vapor growth v in clouds are needed to produce vigorous electrification in the main (i.e., negative) charging zone of thunderstorms. This model applies to collisions between dry surfaces in which one is sharper than the other; thus it explains the negative charging regime ($\Delta Q < 0$) in which the graupel is relatively smooth (Takahashi, 1978), which is $T < 10^\circ\text{C}$ and cloud liquid water contents $\rho_l \sim 0.3 - 3 \text{ g m}^{-3}$ (Fig. 6c). Takahashi's complete data set, which is consistent with the later studies of Pereyra et al. (2000) and Takahashi and Miyawaki (2002), successfully models thunderstorms (Helsdon et al., 2001) and shows that the tripolar nature of thunderstorms arises in part from the boundary in $T - \rho_l$ space between negative and positive graupel charging. Due to the “knob-bly” shape of graupel, precise surface conditions are un-

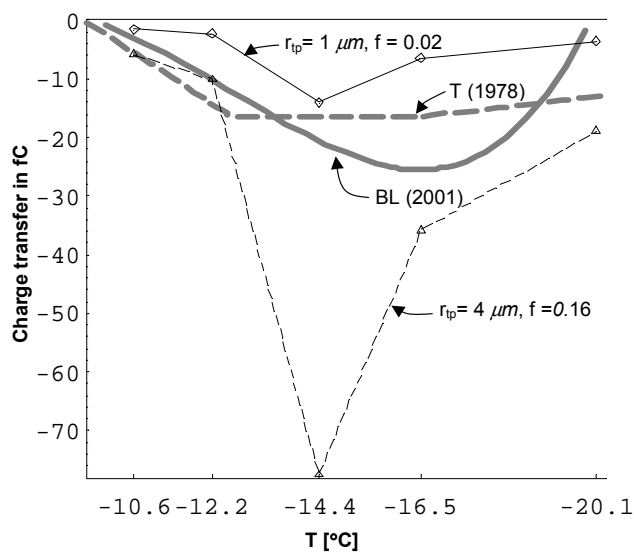


Fig. 5. Predicted charge transfers (Eq. 19) vs data from Takahashi (thick grey, dashed T, 1978) and Berdeklis and List (thick grey, solid BL, 2001) under simulated thunderstorm conditions. Curve T (1978) was made by drawing a line at $\rho_l = 1.1 \text{ g m}^{-3}$ in Fig. 8 of that reference and linking the resulting contour crossing values by straight lines. BL (2001) is the curve fit to data for conditions under liquid water saturation in Berdeklis and List (2001). Calculations used $U = 5.3 \text{ m s}^{-1}$, with measured crystal masses (converted to R_{cr}) and measured growth rates after 3 min of growth from Takahashi et al. (1991). (Measured growth rates were divided by $\sqrt{2}$ because the corners grow slower than the measured points on the crystals.) For the 5 temperatures plotted here, warm to cold, we used growth rates v [$\mu\text{m s}^{-1}$] and R_{cr} [μm] of (0.12, 35.6), (0.16, 40.6), (0.91, 46.4), (0.31, 45.5), and (0.13, 36.4). The maximum thickness of the transferred mass was $\approx 0.5 \mu\text{m}$ and $\theta < 0.68$. The minimum thickness was $\approx 0.28 \mu\text{m}$ at -20°C for $f = 0.02$.

known; but estimates in Williams et al. (1991) indicate that the graupel surface 1. has vapor-grown frost due to the relatively low surface temperature at the lowest ρ_l values (regime of mostly positive charging), 2. sublimates due to the relatively high surface temperature on the graupel at middling ρ_l values (mostly negative charging), and 3. has liquid water at the highest ρ_l values (positive charging). At high ρ_l , the graupel's liquid film would greatly soften the collision, and the dry, cooler surface of a rebounding crystal should instead remove charged liquid from the graupel (Fig. 6d). This should produce overall positive charging (Takahashi, 1978; Graciaa et al., 2001), even if most crystals stick to the graupel. Conversely, positive charging at low ρ_l should result if the frost has the sharper point at the collision (Fig. 6a) or if ice breaks off the graupel (Fig. 6b). In the former case, Eq. (19) would apply with the opposite sign, but fracture, which does occur in the positive regime at low ρ_l , removes much larger amounts of negative charge (Hallett and Saunders, 1979). A maximum amount of charge when a fractured surface is removed from graupel is estimated by multiplying the charge per area in Eq. (14) by the surface area of the fast-

growing frost surface and neglecting any neutralizing H_3O^+ in the interior of the ice (Fig. 2). This amount can exceed -10^4 fC . Thus, even if only a small fraction of the collisions result in fracture, the fractured pieces can dominate the average charge transfer. Our model is consistent with the negative charging regime in thunderstorms and suggests a change to positive at higher and lower ρ_l (entry 8, Table 1b). Therefore, the model here describes a plausible mechanism of thunderstorm electrification.

In addition to the noninductive charge transfer described above, charges induced on ice particles by the in-cloud electric field can also be transferred from particle to particle. This ice-ice inductive charge transfer increases the thunderstorm charging rate after the noninductive ice crystal-graupel mechanism establishes a strong field (Helsdon et al., 2001). Previously, researchers have assumed that these induced charges are transferred by conduction during brief, melt-free collisions (e.g., Illingworth and Caranti, 1985). Given the brevity of such a collisional contact and the relative slowness of conduction, this process has been considered weak. However, if the charge is transferred with melt, as argued here, then ice-ice induction can have greater influence on thunderstorm charging than previously predicted. Also, the melt can soften the collision by limiting the collision pressure to P_{melt} . This can increase collisional contact times, thus increasing the charge conducted during the collision. Moreover, contact times should increase with decreasing r_{ip} due to the smaller contact area, which allows more charge to conduct to snow crystals than that to ice spheres. Thus, charge transfer accompanying mass transfer could partly explain why experiments on ice-ice induction with snow crystals (Scott and Levin, 1970) showed larger charge transfers than the standard inductive theory based on conduction and also larger charge transfers than experiments with ice spheres (Illingworth and Caranti, 1985).

5.2 Effect of impurities on charge transfer

Real ice generally contains impurities, which can affect ice electrical properties. Buser and Aufdermaur (1977) found that NH_3 added to frozen droplets increased their negative charge transfer to a metal target, whereas HF reversed the sign of the transfer (entry 9, Table 1b) and had a larger effect than NH_3 for equal concentrations. To explain these trends, we assume that NH_3 and HF substitute for an H_2O molecule in the ice lattice and the concentration of these impurities is greater in the ice interior than it is on the surface. (The latter is consistent with the tendency of ice to reject impurities and freezing of an ice shell around the droplet before the interior is completely frozen.) The substitution of NH_3 in ice is thought to release an OH^- , leaving a relatively immobile D and NH_4^+ (PW pg. 99). Some of this OH^- should migrate to the surface, which would increase the OH^- concentration at the surface and lead to the observed result. A similar argument holds for NH_4OH , which

would explain results of experiments on sand-ice collisions (Jayaratne, 1991). Conversely, the substitution of HF in ice is thought to release an H_3O^+ and an L, leaving a relatively immobile F^- (PW pg. 98). Some of the H_3O^+ should migrate to the surface, which would increase the H_3O^+ concentration at the surface and lead to the observed result; in addition, migration of L to the surface would produce an electric field that can pull even more H_3O^+ to the surface as in Fig. 1. HCl should have an effect similar to HF but there are as yet no relevant measurements. Measured charging tendencies (Jayaratne, 1991; Jayaratne et al., 1983) with doping of NaCl and $(\text{NH}_4)_2\text{SO}_4$ are qualitatively consistent with our model if one assumes that these compounds dissociate and separate in ice according to measured trends (e.g., Workman and Reynolds, 1950), but quantitative prediction is difficult.

6 Implications of the model to other geophysical and planetary phenomena

In this section, we speculate on the possible roles played by charge redistribution and pressure-melting-assisted charge transfer in nonthunderstorm phenomena.

6.1 Charging between ice and other materials

Non-sublimating ice charges positively when sand particles rebound from it (Jayaratne, 1991). As sand is much harder than ice, charged-mass transfer is predicted to be from the ice surface to the sand and thus should positively charge the ice in agreement with measurement. Also, in the laboratory, ice spheres impacting metals at 10 m s^{-1} deposit net negative charge during rebound, the only exceptions being metals that easily emit electrons from their surface (Buser and Aufdermaur, 1977; Caranti et al., 1985). The hardness of metals allows pressure melting of ice to occur in such collisions (Table 2), and thus the measurements support the present model. Such charging, which can be a nuisance when crystals strike antennas and aircraft (FAA, 2001) or cause corona and sparks from objects in contact with blowing snow (Ives, 1938), should be greatly alleviated if the metal is coated by a thin layer of soft material such as silicone rubber. For example, Table 2 shows that ice crystals would require supersonic speeds to transfer charge to rubber via pressure melting.

6.2 Heterogeneous chemistry

Uptake of tropospheric gases by liquid drops is often highly dependent on pH; however, the effect of intrinsic ice surface pH on surface chemical reactions has not been studied. Charging during growth should make the ice surface more basic due to the high OH^- concentration. For example, if 20 fC of surface charge is contained in a volume $V \approx 3 \mu\text{m}^3$ (typical of data in Fig. 5), the average pH upon melting would be 9.6. The pH right at the surface would likely be greater than this average.

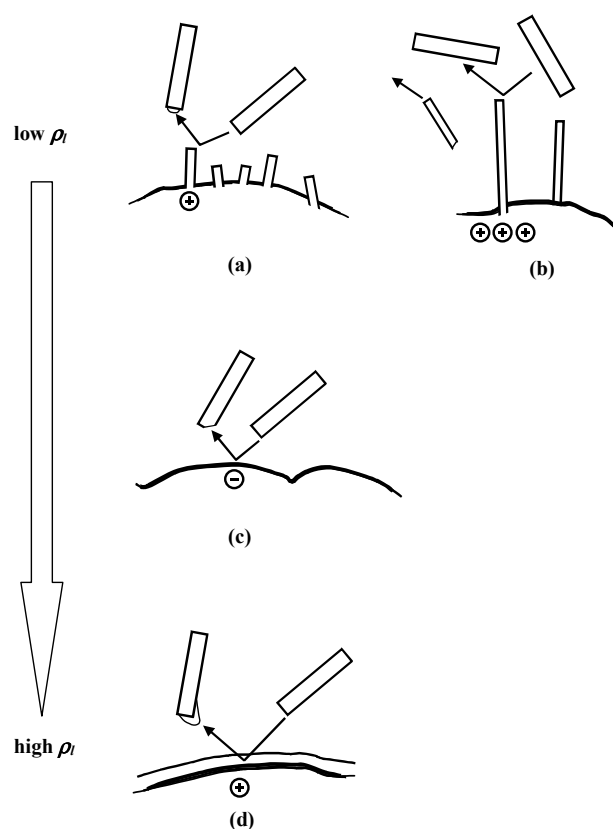


Fig. 6. Mass and charge transfer between vapor-grown crystals, shown as rectangles in motion, and surface regions on graupel, shown at the bottom of each sketch, for low to high ρ_l conditions. a and b occur at low ρ_l when frost, sketched as rectangular spikes, grows on the graupel surface. In a, the negative charge at the corner of the frost transfers to the crystal facet by the same process as in case c except the direction of mass transfer is reversed. If the frost breaks off, as in case b, much more negative charge is removed than in case a. If the crystal instead strikes a smooth, frost-free region (not shown), negative charge transfer occurs just as in case c. In c, the atmosphere has middling values of liquid water content ρ_l and thus the graupel is sublimating due to the latent heating from freezing drops on the surface (not shown). This case is equivalent to that in Fig. 4. Case d is for sufficiently high ρ_l that the graupel has a layer of liquid water. For the rare crystal that does not stick, positive charging occurs because the outermost, negatively-charged, surface of the water layer attaches to the crystal (Takahashi, 1978; Graciana et al. 2001). This direction of mass transfer might also occur when the graupel is dry but very close to 0°C . When the ice crystals are sublimating, the charging in a and c should change sign from those shown in the figure.

6.3 Crystal aggregation

Consequences of surface charging and pressure melting during collisions are largely ignored in atmospheric and planetary studies even though both phenomena can significantly influence various phenomena in these fields. For example,

maximum snowflake size increases dramatically for snowfalls above about -10°C with a smaller peak near -12°C . The apparent increase of collection efficiency at high temperatures has generally been ascribed to inherent surface melting of ice (e.g., Pruppacher and Klett, 1980, p. 502) even though the disordered layer is thought to be only a few nanometers thick for temperature below about -2°C (PW, p. 246). The pressure-melting hypothesis proposed here has a similar temperature versus melt-thickness trend, but the amount of melt can be larger, even for typical collision speeds of snow crystals of $\sim 5\text{ cm s}^{-1}$ (cf. Table 2).

In addition to the role of aerodynamic forces that is often mentioned in discussions of snow crystal aggregation, the aggregation of snow crystals into snowflakes should depend on electrostatic forces between the crystals (Smith-Johannsen, 1969). Furthermore, because collisions transfer only a fraction of the surface charge, collisions involving the tip of one crystal and a non-tip part of another can retain strong electrostatic attraction even after transferring some charged-mass. Thus, the growth charging in this model might partly explain why such point adhesions of two snow crystals are common (Smith-Johannsen, 1969; Finnegan and Pitter, 1988; Kajikawa et al. 2000). A rough demonstration of the possible electrostatic forces follows. Consider two columnar crystals $100\text{-}\mu\text{m}$ long, $20\text{-}\mu\text{m}$ -across, and separated by a gap of 0.5 mm in a “broken-T” orientation (like this:|–). If we ignore the D and L defects and assume that the net OH^{-} charge at the tips are $8 \times 10^{-3}\text{ C m}^{-2}$ (i.e., the predicted charge from Eq. (14) for growth near -15°C) and the compensating H_3O^{+} charges are in the centers of the crystals to make the crystals electrically neutral, then the resulting attractive force is more than twice the gravitational force on each crystal, even for this large separation. Of course, the D and L charges should significantly reduce this attraction; nevertheless, there is a potentially large influence on snowflake formation from surface charging.

In addition, such an electrostatic attraction can be high for fast-growing frost crystals, even at very low temperatures. This attraction likely explains the fragile “yukimorimo” frostballs that form in Antarctica on the snow surface when light winds break rapidly-grown frost crystals that tumble about and clump together (Kameda et al., 1999). Even at low temperatures, growth charging and pressure melting might influence the aggregation of water-frost covered particles in planetary rings (Jurac et al., 1995) and in planetesimal formation.

6.4 Ferroelectric ice grains

Ice grains in snowpacks are often subjected to temperature gradients that allow sublimation on the warmer side of an air gap and growth on the colder side. According to our model, growth polarizes the lattice with an electric field in one direction, whereas sublimation polarizes in the opposite direction (relative to the surface). Thus, such ice grains can partly po-

larize from the growing to sublimating ends, which means that the ice becomes partly hydrogen-ordered and ferroelectric along the average temperature gradient. Raman spectroscopy and inelastic neutron scattering on ice from Antarctica, which originated as snowpack, showed proton ordering in samples kept below 237 K (Fukazawa et al., 1998). Such ordering has been a mystery because solid ice in the laboratory transforms to the hydrogen-ordered XI phase only below 72 K ; but the growth-sublimation of small grains at low temperature might cause such an orientation to freeze into the lattice and remain until the ice is warmed enough for the Bjerrum defects to migrate back to their usual disordered state. Hence, this surface charging might partly explain the hydrogen ordering in Antarctic ice.

In addition, experimental evidence for ferroelectric ice has created a mystery in ice physics because the theoretical ice Ih structure with lowest energy is antiferroelectric (PW, p. 261). One solution to this mystery is the influence of the substrate on ferroelectric ordering in ice films (e.g., Su et al. 1998). The theory here indicates that growth of the ice-vapor interface can also promote ferroelectric ordering; thus, this theory provides another possible solution to the ice physics mystery.

7 Discussion

The fundamental reason why charging occurs in our model is because the positively-charged majority carrier (D) is less mobile than the negatively-charged majority carrier (L) and the resulting build-up of D defects at the surface during growth causes OH^{-} to also build-up at the surface. Thus, our main conclusion is that the interaction between Bjerrum and ionic defects might explain a wide range of experimental results and have broad applications.

However, doing more precise, quantitative modeling of ice charging in the atmosphere is enormously difficult due to the complex nature of ice crystal growth from the vapor, the four types of charge carriers in ice, and because the atmospheric environment includes updrafts, electric fields, water droplets, and various free charges. The nature of the ice surface is itself the source of much debate, the microscale structure of rimed surfaces is unknown, and the collisional process will likely be poorly understood for some time. These complexities justify our simplification of the problem, but it means that the present theory will likely evolve as finer experimental and theoretical details become known. Some details, such as the depth distributions of the charges, the screening of the electric field at the surface by L defects, and non-zero mobility of D might reduce the ionic charging predicted at the outermost surface layer. In contrast, lateral repulsion of charges at the growing surface (and electrical induction before impact) should push (and pull) more charge to the collision points at the corners and thus might greatly increase collisional charge transfer. Growth itself might further increase the charging because the increase of electric field within the

Table 3. List of constants and variables used in the text

symbol	meaning	value [units]	source
A	surface area for mass loss at corner	[m ²]	Fig. 4
d	total D concentration	[m ⁻³]	Eq. (1)
d_0	equilibrium D concentration	[m ⁻³]	Eq. (5)
$d_0(0)$	equilibrium D concentration at surface ($x=0$)	$3 \times 10^{27} \text{ m}^{-3}$	1
D	maximum crystal dimension	[m]	Fig. 2
D_{OH}	OH ⁻ diffusion constant	$1.1 \times 10^{-9} \text{ m}^2 \text{ s}^{-1}$	2*
e	elementary electron charge	$1.6 \times 10^{-19} \text{ C}$	
E	electric field	[V m ⁻¹]	Eq. (3)
f	collision energy fraction for melt transfer	$\sim 0.01\text{--}1.0$	Eq. (17)
F_B	Bjerrum defect creation rate per volume	[m ⁻³ s ⁻¹]	Eq. (1)
F_I	Ionic defect creation rate per volume	[m ⁻³ s ⁻¹]	Eq. (2)
h^-	OH ⁻ volume concentration in ice	[m ⁻³]	Eq. (2)
h^+	H ₃ O ⁺ volume concentration in ice	[m ⁻³]	Eq. (2)
j_D	molecular flux of D defects	[m ⁻² s ⁻¹]	Eq. (1)
j_{OH}	molecular flux of OH ⁻	[m ⁻² s ⁻¹]	Eq. (3)
k	Boltzmann's constant	$1.38 \times 10^{-23} \text{ J K}^{-1}$	
K_0	0th order mass transfer coefficient	$6.71 \times 10^{-3} \text{ C Kg}^{0.5} \text{ m}^{-3.5}$	Eq. (19)
K_1	1st order mass transfer coefficient	$2.1 \times 10^6 \exp[1.14 \times 10^4 (1/T[\text{K}] - 1/253.15)] \text{ C Kg}^{0.5} \text{ m}^{-4.5} \text{ s}$	Eq. (19)
l	L concentration	[m ⁻³]	Eq. (1)
P_0	atmospheric pressure	$\sim 1 \times 10^5 \text{ Pa}$	Fig. 4
P_{con}	pressure at tip of ice during collision	[Pa]	Eq. (15)
P_{melt}	equilibrium melting pressure	[Pa]	Eq. (16)
q_D	effective charge of D defect in ice	$0.38 e$	2
q_L	effective charge of L defect in ice	$-0.38 e$	2
q_{OH}	effective charge of OH ⁻ ion in ice	$-0.62 e$	2
Q	total ionic charge separated within crystal	[C]	Fig. 2
r_{tp}	ice crystal radius of curvature at contact	[m]	Fig. 4
R_{cr}	radius of ice crystal with same volume	[m]	Eq. (15)
T	temperature of the ice	[K]	
U	collision speed	[m s ⁻¹]	Eq. (15)
v	growth speed	[m s ⁻¹]	§3
V	volume of melt transferred in a collision	[m ³]	Fig. 4
x	coordinate for distance from surface	[m]	Eq. (1)
$\langle h \rangle$	mean bulk concentration of H ₃ O ⁺ and OH ⁻	$3 \times 10^{15} \text{ m}^{-3}$	2*
$\langle l \rangle$	mean bulk concentration of L and D	$3 \times 10^{21} \text{ m}^{-3}$	2*†

ice surface can increase the defect creation rates (Onsager, 1934). Similarly, Dash et al. (2001) argued that growth itself produces defects via a disordered growth mechanism that leads to net negative surface charge. Charging is likely to also be aided by the surface forces that tend to push D to the outermost surface layer (Fletcher, 1968). Moreover, partial disorder of the ice-vapor interface, which is predicted to increase with surface charge (PR), allows greater charged-melt transfer than that proposed here. Nevertheless, our theory is based on established properties of ice and is broadly consistent with a wide range of observations. It gives semiquantitative agreement with experiments that, when used in a cloud model, successfully simulate thunderstorm charging.

Similar analysis can be applied to melt growth when more data on the electrical properties of the ice-melt interface become available. Also, other hydrogen-bonded crystals have ionic and Bjerrum defects (Tonkonogov, 1998) and thus might have surface charging similar to that in ice. Examples include many minerals, and NH₃ and H₂S crystals, which are common in the atmosphere of the outer planets. Asymmetry between their contacting surfaces is important whether or not pressure melting occurs. For example, collisions can fracture sharp crystal corners, which can lead to large-scale charge separation via gravitational sedimentation. Thus, the surface charging of hydrogen-bonded crystals such as ice by the motion of Bjerrum defects could have widespread implications.

Table 3. continued

ϵ_0	permittivity of the vacuum	$8.85 \times 10^{-12} \text{ C}^2 \text{ N}^{-1} \text{ m}^2$	
ϵ_s	static dielectric constant of ice	100	3
ϵ_∞	high frequency dielectric constant of ice	3.16	3
δd	change of d due to growth or sublimation	$[\text{m}^{-3}]$	Eq. (7)
δE	change of E due to growth or sublimation	$[\text{V m}^{-1}]$	Eq. (11)
$\delta \phi_{surf}$	surface potential change caused by growth	$[\text{V}]$	§3
δh^-	change of h^- due to growth or sublimation	$[\text{m}^{-3}]$	Eq. (10)
δj_{OH}	change of j_{OH} due to growth or sublimation	$[\text{m}^{-2} \text{ s}^{-1}]$	Eq. (10)
$\delta \sigma$	change of σ due to growth or sublimation	$[\text{C m}^{-2}]$	Eq. (13)
$\delta \sigma_D$	change of σ_D due to growth or sublimation	$[\text{C m}^{-2}]$	Eq. (8)
Δ_D	thickness of high-D region during growth	$[\text{m}]$	Eq. (5)
Δ_{OH}	thickness of high- OH^- region during growth	$[\text{m}]$	Eq. (12)
ΔQ	total charge transferred in a collision	$[\text{C}]$	Eq. (19)
ΔQ_0	equilibrium charge transferred in a collision	$[\text{C}]$	Eq. (18)
ΔQ_v	nonequilibrium charge transfer	$[\text{C}]$	Eq. (19)
μ_L	mobility of L in ice	$0.9\text{--}2 \times 10^{-8} \text{ m}^2 \text{ V}^{-1} \text{ s}^{-1}$	2*†, 4*
μ_{OH}	mobility of OH^- in ice	$3\text{--}8 \times 10^{-8} \text{ m}^2 \text{ V}^{-1} \text{ s}^{-1}$	2*, 4*
θ	interior angle of cone for mass loss at corner	$[\text{rad}]$	Fig. 4
ρ_i	mass density of ice	920 Kg m^{-3}	5*
ρ_l	liquid water content	$[\text{g m}^{-3}]$	§5.1
σ	ionic surface charge	$[\text{C m}^{-2}]$	Eq. (14)
σ_0	ionic surface charge in equilibrium	$[\text{C m}^{-2}]$	Eq. (14)
τ_B	time scale for D and L recombination	$[\text{s}]$	Eq. (1) & (9)
τ_I	time scale for OH^- and H_3O^+ recombination	$[\text{s}]$	Eq. (2)

1. PR

2. PW p. 154

3. Johari (1981)

4. Bryant (1967)

5. PW p. 23

* Estimated value at -20°C

† Estimated activation energy 0.73 eV

‡ Higher value used in computations with activation energy 0.25 eV

Acknowledgements. Charles Knight of NCAR made numerous suggestions for improvement including the interpretation of yukimurimo formation, Clive Saunders of UMIST found several errors in an early version and suggested comparison to measured surface potentials and sublimating ice, and Tsutomu Takahashi of Obirin University made several helpful clarifications. MBB is grateful for the support of the Bosack-Kruger Foundation and also for NSF grant ATM-0211247.

References

- Baker, B., Baker, M. B., Jayaratne, E. R., Latham, J., and Saunders, C. P. R.: The influence of diffusional growth rates on the charge transfer accompanying rebounding collisions between ice crystals and soft hailstones, *Q. J. R. Meteorol. Soc.* 113, 1193–1215, 1987.
- Berdeklis, P. and List, R.: The ice crystal-graupel collision charging mechanism of thunderstorm electrification, *J. Atmos. Sci.* 58, 2751–2770, 2001.
- Bryant, G. W.: Thermoelectric Power of Single Crystals of Ice containing HF or NH_3 , *Phil. Mag.* 16, 495–504, 1967.
- Buser, O. and Aufdermaur, A. N.: Electrification by collisions of ice particles on ice or metal targets, in *Electrical Processes in the Atmosphere*, Dolezalek, H. and Reiter, R. (Eds), Steinkopf, Darmstadt, Germany, 1977.
- Caranti, J. M. and Illingworth, A. J.: Surface potentials of ice and thunderstorm charge separation, *Nature* 284, 44–46, 1980.
- Caranti, J. M., Illingworth, A. J., and Marsh, S. J.: The Charging of Ice by Differences in Contact Potential, *J. Geophys. Res. D* 90, 6041–6046, 1985.
- Castle, G. S. P.: Contact charging between insulators, *J. Electrostatics* 40&41, 13–20, 1997.
- Dash, J. G., Mason, B. L., and Wettlaufer, J. S.: Theory of collisional charging of ice: Microphysics of thunderstorm electrification, *J. Geophys. Res.* 106, 20 395–20 402, 2001.
- Dong, Y. and Hallett, J.: Charge Separation by Ice and Water Drops During Growth and Evaporation, *J. Geophys. Res.* 97, 20 361–20 371, 1992.
- FAA Aeronautical Information Manual: Section 5 (Potential flight hazards), Subsection 7-5-10 (Precipitation static), <http://www>.

- faa.gov/atpubs/aim/Chap7/aim0705.html, 2001.
- Fifolt, D. A., Petrenko, V. F., and Schulson, E. M.: Preliminary study of electromagnetic emissions from cracks in ice, *Phil. Mag. B* 67, 289–299, 1992.
- Finnegan, W. G. and Pitter, R. L.: A postulate of electric multipoles in growing ice crystals: their role in the formation of ice crystal aggregates, *Atmos. Res.* 22, 235–250, 1988.
- Fletcher, N. H.: Surface structure of water and ice II: a revised model, *Phil. Mag.* 18, 1287–1300, 1968.
- Fukazawa, H., Mae, S., Ikeda, S., and Whalley, E.: Proton ordering in Antarctic ice observed by Raman and neutron scattering, *Chem. Phys. Lett.* 294, 554–558, 1998.
- Gaskell, W. and Illingworth, A. J.: Charge transfer accompanying individual collisions between ice particles and its role in thunderstorm electrification, *Q. J. Roy. Meteorol. Soc.* 106, 841–854, 1980.
- Gibbard, S., Levy, E. H., and Lunine, J. I.: Generation of lightning in Jupiter's water cloud, *Nature* 378, 592–595, 1995.
- Graciaa, A., Creux, P., Lachaise, J., and Schechter, R. S.: Charge transfer between colliding hydrometeors: Role of surface tension gradients, *J. Geophys. Res. D* 106, 7967–7972, 2001.
- Hallett, J. and Saunders, C. P. R.: Charge Separation Associated with Secondary Ice Crystal Production, *J. Atmos. Sci.* 36, 2230–2235, 1979.
- Helsdon, J. H., Wojcik, W. A., and Farley, R. D.: An examination of thunderstorm charging mechanisms using a two-dimensional storm electrification model, *J. Geophys. Res.* 106, 1165–1192, 2001.
- Higa, M., Arakawa, M., and Maeno, N.: Size Dependence of Restitution Coefficients of Ice in Relation to Collision Strength, *Icarus* 133, 310–320, 1998.
- Illingworth, A. J.: Charge separation in thunderstorms: small scale processes, *J. Geophys. Res.* 90, 6026–6032, 1985.
- Illingworth, A. J. and Caranti, J. M.: Ice Conductivity Restraints on the Inductive Theory of Thunderstorm Electrification, *J. Geophys. Res. D* 90, 6033–6039, 1985.
- Ives, R. L.: Weather Phenomena of the Colorado Rockies, *J. Franklin Inst.* 226, 691–755, 1938.
- Jaccard, C.: Thermoelectric effects in ice crystals I. Theory of the steady state, *Phys. Kondens. Materie* 1, 143–151, 1964.
- Jayarathne, E. R.: Charge separation during the impact of sand on ice and its relevance to theories of thunderstorm electrification, *Atmos. Res.* 26, 407–424, 1991.
- Jayarathne, E. R., Saunders, C. P. R., and Hallett, J.: Laboratory studies of the charging of soft-hail during ice crystal interactions, *Quart. J. R. Met. Soc.* 109, 609–630, 1983.
- Johari, G. P.: The Spectrum of Ice, *Contemp. Phys.* 22, 613–642, 1981.
- Jurac, S., Baragiola, R. A., Johnson, R. E., and Sittler, E. C., Jr.: Charging of ice grains by low-energy plasmas: Application to Saturn's E ring, *J. Geophys. Res. A* 100, 14 821–14 831, 1995.
- Kajikawa, M., Kikuchi, K., Asuma, Y., Inoue, Y., and Sato, N.: Aggregation of needle snow crystals, *Atmos. Res.* 55, 131–138, 2000.
- Kameda, T., Hoshimi, H., Azuma, N., and Motoyama, H.: Observation of “yukimarimo” on the snow surface of the inland plateau, Antarctica ice sheet, *J. Glaciology* 45, 394–396, 1999.
- Keith, W. D. and Saunders, C. P. R.: Charging of aircraft: high-velocity collisions, *J. Aircraft* 27, 218–222, 1990.
- Kishimoto, Y. and Maruyama, M.: Growth of Ice Ih in Water and Measurements of its Melting Curve, *Rev. High Pressure Sci. Technol.* 7, 1144–1146, 1998.
- Latham, J.: The electrification of frost deposits, *Quart. J. Roy. Meteorol. Soc.* 89, 265–270, 1963.
- Latham, J. and Mason, B. J.: Electric charge transfer associated with temperature gradients in ice, *Proc. Roy. Soc. A*, 260, 523–536, 1961.
- Maeno, N.: Measurements of surface and volume conductivities of single ice crystals, in *Physics and Chemistry of Ice*, Whalley, E., Jones, S. J., and Gold, L. W. (Eds), 140–145, Roy. Soc. Canada, Ottawa, 1973.
- Marshall, B. J. P., Latham, J., and Saunders, C. P. R.: A laboratory study of charge transfer accompanying the collision of ice crystals with a simulated hailstone, *Q. J. R. Met. Soc.* 104, 163–178, 1978.
- Mason, B. L. and Dash, J. G.: Charge and mass transfer in ice-ice collisions: a mechanism for thunderstorm electrification, *J. Geophys. Res.* 105, 10 185–10 192, 2000.
- Martin, J. J., Wang, P. K., Pruppacher, H. R.: A Theoretical Study of the Effect of Electric Charges on the Efficiency with Which Aerosol Particles are Collected by Ice Crystal Plates, *J. Colloid Interface Sci.* 78, 44–56, 1980.
- Odenrantz, F. K. and Buecher, R.: Temperature-Dependence of the Polarity of Electrical Charges on Ice Crystals, *Science* 158, 256–257, 1967.
- Ohtake, T. and Suchanek, R. G.: Electric properties of ice fog crystals, *J. Appl. Meteorol.* 9, 289–293, 1970.
- Onsager, L.: Deviations from Ohm's Law in Weak Electrolytes, *J. Chem. Phys.* 2, 599–615, 1934.
- Pereyra, R. G., Avila, E. E., Castellano, N. E., and Saunders, C. P. R.: A laboratory study of graupel charging, *J. Geophys. Res.* 105, 20 803–20 812, 2000.
- Petrenko, V. F. and Colbeck, S. C.: Generation of electric fields by ice and snow friction, *J. Appl. Phys.* 77, 4518–4521, 1995.
- Petrenko, V. F. and Ryzhkin, I. A.: Surface States of Charge Carriers and Electrical Properties of the Surface Layer of Ice, *J. Phys. Chem. B* 101, 6285–6289, 1997.
- Petrenko, V. F. and Whitworth, R. W.: *Physics of Ice*, Oxford Univ. Press, Oxford, 1999.
- Pruppacher, H. R. and Klett, J. D.: *Microphysics of Clouds and Precipitation*, D. Reidel, Dordrecht, 1980.
- Rydock, J. P. and Williams, E. R.: Charge separation associated with frost growth, *Q. J. R. Meteorol. Soc.* 117, 409–420, 1991.
- Saunders, C. P. R., Peck, S. L., Aguirre Varela, G. G., Avila, E. E., and Castellano, N. E.: A laboratory study of the influence of water vapor and mixing on the charge transfer process during collisions between ice crystals and graupel, *Atmos. Res.* 58, 187–203, 2001.
- Schmidt, R.: Properties of blowing snow, *Rev. Geophys. Space Phys.* 20, 39–44, 1982.
- Scott, W. D. and Levin, Z.: The effect of potential gradient on the charge separation during interactions of snow crystals with an ice sphere, *J. Atmos. Sci.* 27, 463–473, 1970.
- Smith-Johannsen, R. I.: Ice Crystal Agglomeration: T Formation, *J. Atmos. Sci.*, 26, 532–534, 1969.
- Sommer, A. P. and Levin, Z.: Charge transfer in convective thunderclouds induced by molecular interface crossing and free energy reduction, *Atmos. Res.* 58, 129–139, 2001.

- Su, X., Lianos, L., Shen, Y. R., and Somorjai, G. A.: Surface-Induced Ferroelectric Ice on Pt(111), *Phys. Rev. Lett.* 80, 1533–1536, 1998.
- Takahashi, T.: Riming electrification as a charge generation mechanism in thunderstorms, *J. Atmos. Sci.* 35, 1536–1548, 1978.
- Takahashi, T., Endoh, T., Wakahama, G., and Fukuta, N.: Vapor diffusional growth of free-falling snow crystals between -3 and -23°C , *J. Meteorol. Soc. Jpn.* 69, 15–30, 1991.
- Takahashi, T. and Miyawaki, K.: Reexamination of Riming Electrification, *J. Atmos. Sci.* 59, 1018–1025, 2002.
- Tonkonogov, M. P.: Dielectric spectroscopy of hydrogen-bonded crystals, and proton relaxation, *Phys. Uspekhi* 41, 21–48, 1998.
- Vonnegut, B.: Orientation of ice crystals in the electric field of a thunderstorm, *Weather* 20, 310–312, 1965.
- Williams, E. R., Zhang, R., and Rydock, J.: Mixed-phase microphysics and cloud electrification, *J. Atmos. Sci.* 48, 2195–2203, 1991.
- Workman, E. J. and Reynolds, S. E.: Electrical Phenomena Occurring during the Freezing of Dilute Aqueous Solutions and Their Possible Relationship to Thunderstorm Electricity, *Phys. Rev.* 78, 254–259, 1950.